Structure-Based Studies on the Metal-Binding of Two-Metal-Dependent Sugar Isomerases

Ponnandy Prabhu[1,†#], Thi-Ngoc-Thanh Doan[2#], Manish Tiwari[3], Raushan Singh[3], Sun Chang Kim[5], Myoung-Ki Hong[4], Yun Chan Kang[3], Lin-Woo Kang[4,*], Jung-Kul Lee[3,*]

[1]*Department of Bioscience and Biotechnology*, [2]*Department of Advanced Technology Fusion*, [3]*Department of Chemical Engineering,* [4]*Department of Biological Sciences, Konkuk University, 1 Hwayang-Dong, Gwangjin-Gu, Seoul, Korea, 143-701.*

[5]*Department of Biological Sciences, Korea Advanced Institute of Science and Technology, 291 Daehak-ro, Yuseong-gu, Daejeon, Korea, 305-701.*

[†]*Present address: Department of Pathology, The Hebrew University-Hadassah Medical School, Jerusalem 91120, Israel*

[#]These authors equally contributed to this work.

*Corresponding authors:

Jung-Kul Lee, Phone: +82-2-450-3505, FAX: +82-2-458-3504, E-mail: jkrhee@konkuk.ac.kr;

Ling-Woo Kang, Phone: +82-2-450-4090, FAX: +82-2-444-6707, E-mail: lkang@konkuk.ac.kr.

This article has been accepted for publication and undergone full peer review but has not been through the copyediting, typesetting, pagination and proofreading process, which may lead to differences between this version and the Version of Record. Please cite this article as doi: 10.1111/febs.12872

Article type: Original article

Running title: Metal-binding of two-metal-dependent sugar isomerases

Enzymes: L-rhamnose isomerase **EC5.3.1.14,** xylose isomerase **EC 5.3.1.5**

Keywords: *Bacillus halodurans*, crystal structure, isomerase, molecular determinant, rare sugar

Abstract: Two-metal-dependent sugar isomerases are important in the synthesis of rare sugars. Many of their properties, specifically their metal dependency, have not been sufficiently explored. Here we used X-ray crystallography, site-directed mutagenesis, isothermal titration calorimetry, and electron paramagnetic resonance spectroscopy to investigate the molecular determinants of the metal-binding affinity of L-rhamnose isomerase, a two-Mn^{2+} dependent isomerase from *Bacillus halodurans* (BHRI). The crystal structure of BHRI confirmed two metal ion-binding sites: a structural metal ion-binding site for substrate binding and a catalytic metal ion-binding site that catalyzes a hydride shift. One conserved amino acid, W38, in the wild-type BHRI was identified as a crucial residue in structural Mn^{2+} binding, and thus, the catalytic efficiency of BHRI. This function of W38 was explored by replacing it with other amino acids. Its substitution with Phe, His, Lys, Ile, or Ala caused complete loss of the catalytic activity. The role of W38 was further examined by analyzing the crystal structure of the wild-type BHRI and two inactive mutants of BHRI (W38F and W38A) in complex with Mn^{2+}. A structural comparison of the mutants and the wild-type revealed differences in their coordination of Mn^{2+}, including changes in metal-ligand bond length and affinity for Mn^{2+}. The role of W38 was further confirmed in another two-metal-dependent enzyme, xylose isomerase (XI) from *Bacillus*

licheniformis. These data suggest that W38 stabilize protein–metal complexes and in turn aids ligand binding during catalysis in two-metal-dependent isomerases.

Introduction

L-Rhamnose isomerase (L-RhI), an L-rhamnose ketol-isomerase (EC 5.3.1.14), catalyzes the reversible isomerization of L-rhamnose to L-rhamnulose. It can act on a wide range of substrates, isomerizing several sugars to produce sugars that exist infrequently in nature. As such, isomerase enzymes are important for their ability to synthesize rare sugars [1]. These rare sugars, including D-psicose, L-tagatose, L-fructose, D-tagatose, and L-xylulose are of interest in the pharmaceutical and nutritional industries for use as reduced-calorie sweeteners, microbial-growth inhibitors, and bulking agents [2-4]. Nucleoside analogues of L-sugars are also exploited as antiviral drugs against hepatitis-B and HIV, and they could be promising anticancer and cardioprotective agents [5-7]. Moreover, novel L-sugar derivatives have recently been reported to act as inhibitors of urinary glucose reabsorption, suggesting a potential use in the treatment of diabetes [8].

Few L-RhIs have been characterized. L-RhI from *Pseudomonas stutzeri* was shown to have broad substrate specificity, catalyzing the isomerization between L-rhamnose and L-rhamnulose, L-mannose and L-fructose, L-lyxose and L-xylulose, D-ribose and D-ribulose, and D-allose and D-psicose [9]. A gene encoding L-RhI was cloned from *Bacillus pallidus* and characterized [10]. The crystal structure of *P. stutzeri* L-RhI (PSRI, PDB ID: 2HCV), with a resolution of 2.0 Å, was reported in complexes with L-rhamnose and with D-allose, providing insights into its broad substrate specificity [11]. The crystal structure of *Escherichia coli* L-RhI (ECRI, PDB ID: 1D8W), with a resolution of 1.6 Å, was also reported [12]. ECRI exhibited binding to two metal ions; one structural, M1, aids substrate binding, and the other one, catalytic, M2, promotes the

hydride shift. The metal ions have been reported to be Zn^{2+} and Mn^{2+}, respectively [12]. The catalysis of aldose-ketose isomerization by ECRI has been proposed to occur by a metal-mediated hydride shift, where the O1, O2, and O3 atoms of L-rhamnose coordinate with M1 (Zn^{2+}) and M2 (Mn^{2+}). The amino acids K236 and D302, together with the catalytic metal ion (Mn^{2+}) and water, are thought to assist the aldose-ketose isomerization reaction [12].

Mutational studies on xylose isomerase (XI) have been previously performed to improve catalytic efficiency, change its physical properties, and alter substrate specificity [13-16]. Crystallographic and mutational studies on XI not only gave an insight on the structure but also on ligand interaction and reaction mechanisms [17-19]. A number of conserved residues were found to play different roles in interacting with two metal ions (M1, M2) and substrates [20-22]. pH-dependent metal ion binding has been previously studied in xylose isomerase [23-25]. However, systematic analysis of the molecular determinants for metal ion-binding of two-metal-dependent sugar isomerases such as L-RhI has been limited.

The cloning and characterization of L-RhI from *Bacillus halodurans* (BHRI) have been previously reported [26]. Structure-based strategic screening identified a strictly conserved tryptophan (Trp) residue, W38, in BHRI and a position-correlated Trp residue in other two-metal-dependent sugar isomerases, ECRI and PSRI. Its evolutionary conservation indicates its importance in two-metal-dependent sugar isomerases. Therefore, the structural and functional role of this Trp residue was studied in two-metal-dependent sugar isomerases. In this study, the function of W38 was established by X-ray crystallography, site-directed mutagenesis, molecular modeling studies, and thermodynamic titration. W38 was shown to facilitate the proper binding

of the structural metal ion and to aid the binding of the substrate in BHRI. To elucidate the role of W38, X-ray crystal structures with Mn^{2+} and suitable docked substrates were compared. This work systematically identified the molecular determinant for metal-ion binding of two-metal-dependent isomerases.

Results

Overall structure of *B. halodurans* L-RhI (BHRI)

The structure of apo BHRI was determined by the molecular replacement method. Four protomers were found in an asymmetric unit (Fig. 1A). The final model of BHRI was refined to an R_{cryst} of 18.9% and an R_{free} of 25.5%. Analysis by PROCHECK showed that almost all residues in the structures were in allowed regions and less than 2% in generously allowed regions (Table 1). The electron density for all residues was well defined, except for the six His-tag residues, three amino acids at the N-terminus, and one region from L48 to G61, which was called the β1-α1-loop in the ECRI structure. The β1-α1-loop of ECRI has only been shown in substrate bound structures [12]. Like other reported L-RhI structures, each BHRI monomer consisted of two domains, one large domain with eight α-helices, eight β-strands, and one small domain with α-helices at the N-terminus and the C-terminus. The larger domain was called the $(\beta/\alpha)_8$-barrel domain, and it extended from P32 to L353. The smaller helical domain comprised six apical helices: two from the N-terminus to V31 and four from I354 to the C-terminus. Each BHRI monomer had an active site in the center of the barrel domain where two metal ions were found in BHRI-Mn complex structure (Fig. 1B). Structure-based sequence alignment showed that the L-RhI structures of *E. coli* and *P. stutzeri* exhibited similar folding as the BHRI structure, despite having different sequence identities (57% identity to *E. coli* and 14% identity to *P.*

stutzeri) (supplementary Fig. S1). The overall structure of the BHRI tetramer (Fig. 1A) was similar to that of the ECRI tetramer (rmsd = 0.99 Å) in which the loop regions between the β-strands and α-helices of the large domain pointed towards the inside of the tetramer. In ECRI, the β1-α1-loop of Mol-A was oriented to the interface of Mol-A and Mol-C, and it provided two residues for the substrate-binding site in Mol-A only [12].

Substrate binding pocket of BHRI

Two metal ions were observed in the BHRI protomer crystal structure (BHRI-Mn) (Fig. 1B). One structural metal ion (M1) aids substrate binding, and the other catalytic metal ion (M2) promotes the hydride shift (Fig. 2). Based on the crystal structure of ECRI, its metal-ion-binding residues have been previously proposed to be E234, D267, H294, and D334 binding to M1, and H270 and D302 binding to M2. Metal-ion-coordination in BHRI-Mn was also observed. E225, D258, H285, and D325 coordinated with M1, and D258, H261, D293, and D295 coordinated with M2 (Fig. 3). K236 in ECRI, corresponding to K227 in BHRI was confirmed to assist aldose-ketose isomerization through a hydride shift [12].

Sequence and structure-based mapping of critical residues

Conserved residues in the BHRI sequence were identified by multiple sequence alignment with other L-RhI sequences (supplementary Fig. S2). Multiple sequence alignment of 12 L-RhIs revealed 129 amino acids that were fully conserved (100% identical) throughout the sequence. The substrate L-rhamnose was docked into the crystal structure of BHRI-Mn using DS 3.0 (Accelrys Software Inc., San Diego, CA, USA). Twenty amino acid residues, including the six metal-ion-binding residues and K227 were found within 5Å of the substrate-binding pocket

(SBP). Of these 20 residues, 15 were conserved amino acids and five were non-conserved. Among the 15 conserved residues, six were metal-ion-binding residues (E225, D258, H261, H285, D293, and D325) and one was K227. Therefore, the roles of the eight remaining conserved residues (N182, N131, F327, H36, W184, W38, F135, and W292) were further investigated (supplementary Fig. S3).

Alanine substitution of selected residues

To examine the role of the selected conserved residues, each was individually mutated to alanine (Ala). Recombinant enzymes carrying N182A, N131A, F327A, H36A, W184A, W38A, F135A, and W292A mutations were expressed and purified. When their activity was analyzed and compared with the wild-type BHRI, only substitution at W184, W292, and W38 significantly altered L-RhI activity (Table 2). The K_m and k_{cat} values of N182A, N131A, F327A, H36A, and F135A mutants were similar to those of the wild-type enzyme. Mutants W292A and W184A had decreased k_{cat} values, and the W38A mutant was inactive. Thus, position W38 was considered as a crucial determinant of BHRI activity and was further investigated by site-directed mutagenesis.

Analysis of the role of W38 by site-directed mutagenesis and the structure of the BHRI variants

W38 was mutated to non-polar aromatic, non-polar hydrophobic, and polar/charged residues by site-directed mutagenesis. All mutated BHRIs were expressed at levels similar to that of the wild-type BHRI. Mutants W38E, W38D, W38R, W38H, W38K, W38I, W38L, W38Y, and W38F showed no enzymatic activity. The wild-type and mutant BHRI proteins exhibited similar CD spectra, with ellipticity minima of comparable amplitudes in the 220 to 230 nm range (data

not shown). This indicated that all tested wild-type and mutant enzymes had similar secondary structures and that the introduced mutations did not cause major misfolding. Despite their efficient expression and similar secondary structure, the mutants were inactive, demonstrating the crucial role of W38 in catalysis.

To gain molecular insight, crystal structures were determined for wild-type BHRI and two mutants (W38F and W38A) as described in the experimental procedures. In the wild-type BHRI structure, both M1 and M2 metal ions were present (Fig. 3A and supplementary Fig. S4). Metal ion coordination in the BHRI-Mn structure shows that M1 coordinates with E225, D258, H285, D325, and two water molecules. When wild-type BHRI was docked with cyclic L-rhamnose (BHRI-Mn-CyclicRham), putative hydrogen bonding occurred between O2 and O3 of the substrate and the carboxylic side chain of M1-binding residue D325 (Fig. 3B and supplementary Fig. S4). Cyclic L-rhamnose bound to M1. O3 and O4 of the substrate interacted with M1.

In the mutant W38F-Mn structure (Fig. 4A), M1 was coordinated by only five ligands (E225 (bidentate coordination), D258, H285, and D325). No water molecules were bound to M1 metal ion. M2 also lost the coordination from D295. The metal coordination distances were longer than those of the wild-type BHRI-Mn. When W38F-Mn was docked with cyclic L-rhamnose (W38F-Mn-CyclicRham) (Fig. 4B), M1 was not coordinated with O3 or O4 of the cyclic substrate. W38A lacked both M1 and M2 in its binding pocket (supplementary Fig. S5). When the W38A crystal structure was docked with the substrate (W38A-CyclicRham), there was no interaction between L-rhamnose and the W38A structure.

We further compared the apo and metal-bound wild-type structures with W38F-Mn and W38A-Mn structures (Fig. 5). In the W38F-Mn and W38A-Mn structures, the terminal carboxylic side chains of D325 were rotated by approximately 66°, and they lost the coordination to M1 ion. The rotated D325 side chain had new hydrogen bonds with the D295 side chain in both W38F-Mn and W38A-Mn structures, which also caused a loss in the coordination to M2 ion. Accordingly, the mutation of W38 disrupted the coordination of both metal ions.

Stoichiometric analysis of Mn^{2+}

The stoichiometric analysis of Mn^{2+} in the wild-type and mutant BHRIs was performed by inductively-coupled plasma mass spectroscopy (ICP-MS). Mn^{2+} was found at 7.9, 6.1, and 1.0 mol/mol in wild-type BHRI, W38F, and W38A tetrameric enzymes, respectively. This corresponds to two Mn^{2+} ions per wild-type BHRI monomer, less than two ions per W38F monomer, and a negligible amount in the W38A monomer.

Analysis of the functional role of W38 by measuring the thermodynamics of metal binding in BHRI variants

Crystal structure analysis of BHRI-Mn showed that residue W38 is in close proximity to one of the M1-binding residues, D325. The distance between NE1 of W38 and OD1 of D325 is 3.4Å (Fig. 3A), which suggests that the indole ring of W38 is involved in stabilizing the protein-metal ion complex by interacting with D325, in turn aiding substrate binding.

Binding of wild-type and mutant (W38A and W38F) BHRI variants to Mn^{2+} was studied by ITC. The heat output due to enzyme-metal interactions was fitted using the Nano Analyze

software (TA Instruments, New Castle, DE, USA) to calculate the dissociation constant, K_d, and the binding enthalpy, ΔH (Table 3). The binding curves were fitted by a two-site binding equation, assuming a model of independent (i.e., non-interacting) sites (Fig. 6). By Mn^{2+} titration, wild-type BHRI binding affinity for Mn^{2+} (K_d = 1.57 μM) was 5-fold higher than that of W38F (K_d = 8.14 μM) and approximately 466-fold higher than that of W38A (K_d = 732 μM).

General role of W38 in two-metal-dependent isomerases

Further investigation was carried out to understand how W38 affects the catalytic activity of two-metal-dependent sugar isomerases. Different amino acid sequences of the two-metal-dependent sugar isomerases, including L-RhI, XI, and glucose isomerase, were aligned. The W38 residue was completely conserved throughout the sequences (supplementary Fig. S2). Therefore, the W38 residue may be critical in all two-metal-dependent isomerases. To confirm the general role of Trp in two-metal-dependent isomerases, a different class of sugar isomerase, XI, was studied by mutagenesis. The sequence identity of XI with L-RhI was low (less than 10%). Nevertheless, the metal-binding sites were well conserved in both the enzyme sequences and structures (supplementary Fig. S2 and S3). A new sequence of XI from *B. licheniformis* (BLXI) was chosen as a model to be cloned and overexpressed. Sequence alignment identified the W38 residue in BHRI as W47 in BLXI (supplementary Fig. S6). W47 was mutated to Ala or phenylalanine (Phe), and the resulting W47A and W47F BLXI mutants exhibited complete loss of XI activity. This indicates that the Trp residue is likely critical for activity in all two-metal-dependent sugar isomerases.

Discussion

The goal of this study was to identify critical amino-acid residues linking the structure and function of two-metal-dependent isomerases, including BHRI. The mutational studies focused on the conserved residues near the SBP, because such residues often have significant effects on both enzyme structure and function. However, their functions are not well understood. Systematic screening identified the molecular determinants. Multiple sequence alignments allowed us to identify conserved residues and X-ray crystallography followed by substrate docking helped us identify conserved residues in contact with the substrate. Site-directed mutagenesis of individual residues was then undertaken. Molecular docking and mutational analysis of the residues in the SBP of wild-type BHRI showed that W38 could influence substrate binding by stabilizing the M1 via one of the M1-binding residues, D325. The W38A BHRI mutant completely lost enzymatic activity and further mutations at position 38 indicated that W38 is essential for the activity of BHRI. Since W38 is conserved in all two-metal-dependent isomerases, its general role was further confirmed using BLXI, a different two-metal-dependent sugar isomerase. These results suggest that W38 is a crucial determinant not only for L-RhI, but also for all two-metal-dependent sugar isomerases.

Isomerases with a metal ion at the catalytic center act through a hydride shift mechanism [17]. Crystal structures of ECRI and BHRI revealed the presence of two metal ions (M1 and M2). In ECRI, the catalytic amino acids K236 and D302 (K227 and D293, respectively, in BHRI), together with the catalytic metal ion (Mn^{2+}) and water, are thought to assist the aldose-ketose isomerization reaction through a hydride shift mechanism (Fig. 2). Two-metal-dependent isomerase M1 ion is important for substrate binding [11, 12, 19]. Disruption of metal

coordination would have a severe effect on the enzyme activity [27-30]. Decreased amount of Mn^{2+} in the sample was demonstrated through analysis of ICP-MS. The stoichiometric analysis of Mn^{2+} in the wild-type and mutant BHRIs revealed a significant reduction of total Mn^{2+} content in the mutants. This finding strongly suggests that Mn^{2+} is associated with wild-type BHRI, but mutation at W38 diminishes or abolishes metal-binding affinity. The ICP-MS results prompted us to analyze the binding pattern of Mn^{2+} and substrate in the wild-type and mutant BHRIs, to identify differences in the geometrical parameters of the Mn^{2+} coordination in the protein and substrate.

In wild-type BHRI, containing Trp at position 38, cyclic L-rhamnose bound first to M1, which is followed by the linearization of the substrate. The linear L-rhamnose then interacts with M1 and M2 for isomerization via a hydride shift [12]. This is similar to the proposed mechanism for another two-metal-dependent sugar isomerase, XI [19]. Cyclic L-rhamnose was analyzed when docked in the SBP of wild-type BHRI-Mn (Fig. 3B). In wild-type BHRI, M1 was coordinated in an octahedral form with six coordination bonds from E225, D258, H285, D325, and two water molecules (Fig. 3A), indicating a more symmetric octahedral geometry. This geometry may better localize the metal and restrict its mobility for the incoming substrate to bind. In general, all Mn sites are found to present an octahedral coordination geometry [11], which was consistent in wild-type BHRI.

Replacement of Trp with Phe or Ala caused a complete loss of activity. The structure of W38F-Mn (Fig. 4A) showed significant differences in metal-ion coordination when compared with the wild-type enzyme (Fig. 3A). M1 was coordinated with only five coordination bonds

from E225 (bidentate coordination), D258, H285, and D325 (Fig. 4A). Thus, the octahedral coordination geometry of Mn^{2+} was distorted [31-34]. In addition to distorted M1 geometry, the separation of the two metal ions (M1 and M2) was shortened to approximately 3.7 Å in the W38F-Mn structure compared to that of the wild-type, 4.7 Å. The distances between the M1-binding residues (E225, D258, and D325) and M1 were increased compared with those in the wild-type enzyme. These changes confirmed the improper positioning of the metal-ion-binding site, causing improper binding of the cyclic substrate to M1 (Fig. 4B). However, diffraction data of W38A crystals showed that W38A lacked both M1 and M2 in its binding pocket. When Ala was substituted at position 38, the metal-ion-binding site was disoriented. Post-docking analysis of the W38A crystal structure with the substrate (W38A-CyclicRham) confirmed no interaction of the substrate L-rhamnose with the W38A mutant enzyme.

Xylose isomerases, glucose isomerases, rhamnose isomerases and AraC have the α-anomer preference of their substrates, xylose, glucose, rhamnose and arabinose, respectively [12, 17, 35]. It was shown that the α-anomer preference of the substrates is due to the inability of the xylose isomerase to perform the ring opening reaction on the β-xylose [17, 36]. The docking results obtained with BHRI showed that the α-anomer of L-rhamnopyranose was fitted better than the β-anomer in the substrate binding site. The NE2 of His93 is within hydrogen bonding distance of the ring oxygen with 3.6 Å (Fig. 3B) for cyclic α-L-rhamnopyranose. In XI, it was suggested that His54 is involved in catalyzing the sugar ring opening in the reaction mechanism [17] and probably governs the anomeric specificity of the enzyme [20]. The structural equivalent to this histidine residue in BHRI is His93. This suggests that His93 may be involved in catalyzing the sugar-ring opening step in the rhamnose isomerase mechanism [12, 17]. Unlike the wild-type

BHRI, docking of L-rhamnopyranose in W38F showed no possible interaction with His93 (Fig. 4B). However, an X-ray crystal structure of BHRI complexed with L-rhamnopyranose is needed to confirm the docking study and the structural interpretation discussed above.

Calorimetric measurements by ITC (Fig. 6) showed that the binding of Mn^{2+} to mutant W38F was unfavorable compared with the wild-type BHRI (Table 3). The resulting affinities (K_d) of the W38F and W38A mutants for Mn^{2+} were 5- and 466-fold lower than that of the wild-type enzyme, respectively. EPR measurements were carried out to provide additional evidence of metal-ion coordination in wild-type BHRI and mutant W38F. Typically, mononuclear Mn^{2+} centers give rise to an intense g = 2.0 signal with a six-fold nuclear hyperfine splitting due to ^{55}Mn (I = 5/2) [37]. The X-band EPR spectrum of wild-type BHRI presented a signal at g = 2.0 with the six-fold hyperfine splitting (supplementary Fig. S7). A strong EPR signal at g = 2.0 was observed for mutant W38F. In general, Mn^{2+} EPR signals are readily observed when the metal is free in solution, but not when the ion forms a complex with the protein [38]. It is clear that Mn^{2+} was completely coordinated in wild-type BHRI, diminishing the EPR spectra. In contrast, Mn^{2+} in W38F mutant is free, which leads to the strong EPR signal (supplementary Fig. S7). The weak EPR signal in the wild-type BHRI is likely due to the electronic environment of the Mn^{2+} caused by interaction of the Mn^{2+} with the M1-binding residues. This interaction is absent in the W38F mutant. Although Mn^{2+} ions were present in the crystal structure of the wild-type BHRI and the W38F mutant, the coordination patterns were different, as supported by the crystal structure and EPR studies. Similar differences in the EPR spectra of Mn^{2+} derived from single mutation have been reported in catechol dioxygenase from *Arthrobacter globiformis* [39, 40], lactose permease of *E. coli* [38], and phosphofructokinase-2 from *E. coli* [41].

Previous studies suggested that Trp16 in *Streptomyces rubiginosus* XI, corresponding to Trp38 of BHRI excludes solvent from C1 and C2 of the substrate, therefore acting as a hydrophobic barrier, preventing the exchange of the transferred hydrogen with the solvent [17]. Trp 16 (corresponding to W38 of BHRI) in *Actinoplanes missouriensis* XI was shown to be involved in substrate binding rather than catalysis, presumably by maintaining the architecture of the active site mostly by the mere bulk of their side chain [20]. Substitution of Trp49 (corresponding to Trp38 of BHRI) in the *T. thermosulfurigenes* XI with phenylalanine and alanine residues resulted in the loss of activity towards xylose [13].

Tryptophan has a unique role in the folded structure and the binding site of many proteins [42]. Of all the ring atoms in tryptophan, NE1 shows the highest number of interactions, both along the edge (hydrogen bonding) as well as along the face, generating stability to the protein structure and binding site [42, 43]. In wild-type BHRI, OD1 of Asp325 accepts a hydrogen bond from an indole NE1 of the direct ligand Trp38 (Fig. 3A). This interaction is postulated to preorganize the substrate binding site and, thereby, enhance the overall affinity for the active site manganese [44]. The determined crystal structure of W38A is very similar to that of the wild-type enzyme. However, the metal ion binding site and the calorimetric measurements by ITC (Fig. 6) showed a difference in manganese binding. A representative titration of W38A and wild-type with $MnCl_2$ is shown in Figure 6. The mutation resulted in a weak manganese binding (Table 3). The striking feature of manganese binding to W38A is that association of manganese in their affinity site proceeds with an unfavorable change in enthalpy near room temperature [44]. The observed thermodynamic data for W38F and W38A with the second-shell hydrogen bond removed (Fig. 4 and S5) are in significant contrast to those obtained for wild-type BHRI,

suggesting a probably much larger enthalpic role for the tryptophan residue as a second-shell ligand [45-47]. Nonetheless, all of the suggested phenomena likely contribute to the overall net enthalpy of metal ion binding. These data suggest that, in addition to decreasing manganese affinity, Asp325-Trp38 hydrogen bond significantly increases the dissociation rate constant, resulting in the disruption of the manganese coordination to form the octahedral site [44, 48]. The data reported in our study suggest that Trp, a non-metal-coordinating conserved residue, is involved in metal-binding affinity and, therefore, the activity of two-metal-dependent sugar isomerases.

The results of structure-based systematic screening, X-ray crystallography, and thermodynamic analyses suggest that W38 binds to D325 (an M1-binding residue), stabilizes protein–metal complexes, and, in turn, aids ligand binding of two-metal-dependent sugar isomerases (Fig. 3). A general role for W38 was further confirmed with BLXI, a different class of two-metal-dependent sugar isomerase. The reported observations should aid the understanding of the protein/metal partnership in all two-metal-dependent sugar isomerases.

Materials and methods

Materials, bacterial strains, and culture conditions

For PCR, Ex-*Taq* DNA polymerase was purchased from Promega (Madison, WI, USA). Restriction enzymes were obtained from New England Biolabs (Ipswich, MA, USA). pQE-80L expression vector, plasmid isolation kit, and Ni-NTA Superflow purification column were obtained from Qiagen (Hilden, Germany). Oligonucleotide primers were obtained from Bioneer (Daejeon, South Korea). Electrophoresis reagents were obtained from Bio-Rad laboratories

(Hercules, CA, USA) and all assay chemicals were obtained from Sigma-Aldrich (St. Louis, MO, USA). The plasmid containing the wild-type BHRI gene was used to produce the wild-type BHRI protein. Cultures of *E. coli* strains harboring the wild-type and mutant BHRI genes for protein expression were grown at 37°C in Luria-Bertani (LB) medium supplemented with ampicillin (100 μg/mL). Isopropyl-β-D-thiogalactopyranoside (IPTG) was then added to the culture medium at a final concentration of 0.5 mM. Incubation was continued with shaking at 37°C.

Site-directed mutagenesis of BHRI

Site-directed mutagenesis was carried out using a QuikChange site-directed mutagenesis kit from Stratagene (La Jolla, CA, USA). Recombinant plasmid pQE-BHRI containing the wild-type L-RhI gene was used as the DNA template [26]. Plasmids containing the correct mutant genes were then used to transform *E. coli* BL21 (DE3). Colonies selected by ampicillin resistance were used for protein expression.

Purification and protein quantification

Wild-type and mutant enzymes were purified using a previously described procedure [12]. Cell pellets were resuspended in 20 mM sodium phosphate buffer (pH 7.5). The cell suspension was incubated on ice for 30 min in the presence of 1 mg/mL lysozyme. Cells were disrupted by sonication at 4°C for 5 min, and the lysate was centrifuged at 14,000 × *g* for 20 min at 4°C to remove cell debris. The resulting crude extract was retained for purification. The cell-free extract was added to a Ni-NTA Super flow column (3.4 × 13.5 cm, Qiagen) pre-equilibrated with a binding buffer (50 mM NaH_2PO_4, 300 mM NaCl, pH 8.0). Unbound proteins were washed from

the column with a washing buffer (50 mM NaH_2PO_4, 300 mM NaCl, 20 mM imidazole, pH 8.0). The protein was then eluted from the column with an elution buffer (50 mM NaH_2PO_4, 300 mM NaCl, 250 mM imidazole, pH 8.0). Enzyme fractions were analyzed by 12% sodium dodecyl sulfate-polyacrylamide gel electrophoresis (SDS-PAGE) and visualized by staining with Coomassie blue R250. Protein concentrations were determined by the Bradford method using bovine serum albumin as a protein standard [49].

Enzyme assay and determination of kinetic parameters

L-RhI activity was determined by measuring the amount of L-rhamnulose formed. Under standard conditions, the reaction mixture contained 1 mM $MnCl_2$, 15 μg enzyme, 50 mM L-rhamnose (substrate), and 50 mM malate buffer (pH 7) in a final volume of 100 μL. The reaction mixture was incubated at 70°C for 10 min and then cooled on ice to stop the reaction. The generated L-rhamnulose was determined using cysteine carbazole-sulfuric acid, and its absorbance was measured at 560 nm [50]. Isomerization of the substrate and accumulation of product in the reaction mixture were determined by a colorimetric method and high performance liquid chromatography (HPLC, DIONEX, Sunnyvale, CA, USA) using a separation column (NH2P-50 4E, Shodex, Munich, Germany) at 30°C eluted with 75% acetonitrile at a flow rate of 0.5 mL/min. One unit of L-RhI activity was defined as the amount of enzyme required to catalyze the formation of 1 μmol keto-sugar per min under the above-specified conditions.

Data collection and structure determination

Crystals of BHRI wild-type and mutants W38F and W38A were produced by the hanging drop method [51]. Briefly, crystals were grown for 1 week using a reservoir solution of 10% (w/v)

PEG 8000, 0.1 M HEPES pH 6.0 and 0.2 M sodium acetate in a 24-well plate. Crystals of metal complexes were obtained by soaking $MnCl_2$ in the drop containing BHRI crystals and incubating for 12 h. The crystals were flash-cooled in liquid nitrogen before data collection. Diffraction data for all structures were collected on beam lines of 4A and 6C1 at the Pohang Light Source (PLS, Republic of Korea) using a Bruker Proteum 300 CCD detector. The data were indexed, integrated and scaled via the DENZO and SCALEPACK [52]. The initial structure of apo BHRI was determined by molecular replacement using MOLREP [53] from the CCP4 program package with a template of L-RhI from *E. coli* (ECRI) (PDB ID: 1d8w). The initial R-factor from the resulting model was 39.3%, which produced a clearly-interpretable electron density map of the overall structure. Further refinement was performed by REFMAC5. After each round of refinement, model building was performed using Coot 0.5.2. Water molecules were added where stereochemically plausible. Metal ions were assigned to positions where the electron density was too high to be explained by water. The quality of the model was checked by PROCHECK in the CCP4 program package [54]. The structures of BHRI-Mn, W38F-Mn, and W38A were determined using MOLREP [53] with the apo BHRI structure as a template. Isotropic B-factors were refined in all structures and analyzed using the CCP4 program suite. The data collection and refinement statistics are summarized in Table 1.

Structure analysis

Results were analyzed using X-ray crystal structures with suitable docked substrates. These were wild-type enzyme with Mn^{2+} (BHRI-Mn), wild-type enzyme with Mn^{2+} and L-rhamnose docked in its cyclic form (BHRI-Mn-CyclicRham), mutant W38F with Mn^{2+} (W38F-Mn), mutant W38F with Mn^{2+} and L-rhamnose docked in its cyclic form (W38F-Mn-CyclicRham), and mutant

W38A with L-rhamnose docked in its cyclic form (W38A-CyclicRham). The substrate was docked into the SBP of wild-type and mutant structures using C-DOCKER, a molecular dynamics simulated-annealing-based algorithm module from Discovery Studio (DS) 3.0 (Accelrys Software Inc., San Diego, CA, USA). Different poses were created using random rigid-body rotations followed by simulated annealing [55]. Before docking, the structures of the protein, substrate, and their complexes were subjected to energy minimization using CHARMM forcefield as implemented in DS 3.0. A full-potential final minimization was then used to refine the substrate (ligand) poses. The substrate orientation that gave the lowest interaction energy was chosen for further rounds of docking. Based on the C-DOCKER energy, the docked conformation of the substrate was retrieved for post docking analysis.

Isothermal titration calorimetry (ITC)

The binding of Mn^{2+} to wild-type and mutant BHRIs was monitored by ITC. Titrations were performed on a Nano ITC low-volume titration calorimeter (TA instruments, New Castle, DE, USA). In a typical ITC experiment, $MnCl_2$ (10 mM) was titrated with wild-type BHRI (0.08 mM) or the mutants, W38A (0.1 mM) or W38F (0.09 mM). The instrument was equilibrated at 25°C until the baseline was flat and stable. The titration data were analyzed using Nano Analyze software (TA Instruments) using an independent model to obtain the fitting graph and thermodynamic binding data [27]. The binding intrinsic molar enthalpy change (ΔH), binding stoichiometry (n), and binding constant (*K*) were obtained from fitting the calorimetric data. Changes of the binding Gibbs free energy (ΔG) and entropy (ΔS) were calculated from K and ΔH using the following fundamental equations: $\Delta G = -RT \ln K$ and $\Delta S = (\Delta H - \Delta G)/T$. All experiments were performed in 50 mM malate buffer with stirring at 300 rpm.

Electron paramagnetic resonance spectroscopy

Electron paramagnetic resonance (EPR) spectra were recorded at X-band (9.2 GHz) on a Bruker BioSpin spectrometer using a standard rectangular Bruker EPR cavity equipped with an Oxford helium flow cryostat (ESR 900). The magnetic field was measured using a Bruker gaussmeter (ER035M) and the spectra were taken at 295 K by using 2.5 G modulation, and 2 mW microwave power. The EPR samples were prepared in solutions buffered to pH 7.0 with 50 mM malate buffer. The protein concentration for wild-type and mutant were 0.3 mM. Before the samples were analyzed, the enzymes were treated with 1 mM Mn^{2+} and thoroughly dialyzed with 50 mM malate buffer.

Analytical methods and protein database search

Optical spectra were recorded on a Varian Cary 100 Bio UV-Vis spectrophotometer (Palo Alto, CA, USA). Amino-acid sequences deduced from the *L-RhI* gene sequences of *Bacillus halodurans* were compared with those of related enzymes from other sources using the BLAST network at the National Center for Biotechnology Information. Multiple sequence alignment was performed using the ClustalW program.

PDB accession number

Atomic coordinates and structural factors of BHRI, BHRI-Mn complex as well as W38F and W38A BHRI mutants were deposited in the PDB under PDB code 3P14, 3UU0, 3UVA, and 3UXI, respectively.

Acknowledgements

This research was supported by the Converging Research Center Program through the National Research Foundation of Korea (2011-50210), and a grant from the Intelligent Synthetic Biology Center of Global Frontier Project (2011-0031955) funded by the Ministry of Science, ICT and Future Planning, Republic of Korea. This work was also supported by the Energy Efficiency & Resources Core Technology Program of the Korea Institute of Energy Technology Evaluation and Planning (KETEP), granted financial resource from the Ministry of Trade, Industry & Energy, Republic of Korea (201320200000420).

Author contribution

J.K.L., L.W.K., P.P. and T.N.T.D. designed the research, analyzed the data and wrote the paper. P.P., T.N.T.D., M.T., R.S., S.C.K., Y.C.K., and M.K.H. performed the experiments. P.P. and T.N.T.D. contributed equally to this work.

References

1. Izumori, K. (2002) Bioproduction strategies for rare hexose sugars, *Naturwissenschaften.* **89**, 120-4.
2. Bautista, D. A., Pegg, R. B. & Shand, P. J. (2000) Effect of L-glucose and D-tagatose on bacterial growth in media and a cooked cured ham product, *J Food Prot.* **63**, 71-7.
3. Lawson, C. J., Homewood, J. & Taylor, A. J. (2002) The effects of L-glucose on memory in mice are modulated by peripherally acting cholinergic drugs, *Neurobiol Learn Mem.* **77**, 17-28.

4. Livesey, G. & Brown, J. C. (1995) Whole body metabolism is not restricted to D-sugars because energy metabolism of L-sugars fits a computational model in rats, *J Nutr.* **125**, 3020-9.
5. Kasiganesan H, W. G., Chiacchio MA, Gumina G (2009) Novel L-adenosine analogs as cardioprotective agents, *Bioorg Med Chem.* **17**, 5347-52.
6. Mathé C, G. G. (2006) L-Nucleoside enantiomers as antivirals drugs: a mini-review, *Antiviral Res.* **71**, 276-81.
7. Fishman P, B.-Y. S., Madi L, Cohn I (2002) A3 adenosine receptor as a target for cancer therapy, *Anti-Cancer Drugs* **13**, 437-43.
8. Goodwin NC, M. R., Harrison BA, Shadoan MK, Almstead ZY, Xie Y, Healy J, Buhring LM, DaCosta CM, Bardenhagen J, Mseeh F, Liu Q, Nouraldeen A, Wilson AG, Kimball SD, Powell DR, Rawlins DB (2009) Novel L-xylose derivatives as selective sodium-dependent glucose cotransporter (SGLT2) inhibitors for the treatment of type 2 diabetes, *J Med Chem.* **52**, 6201-4.
9. Leang, K., Takada, G., Ishimura, A., Okita, M. & Izumori, K. (2004) Cloning, nucleotide sequence, and overexpression of the L-rhamnose isomerase gene from *Pseudomonas stutzeri* in Escherichia coli, *Appl Environ Microbiol.* **70**, 3298-304.
10. Poonperm, W., Takata, G., Ando, Y., Sahachaisaree, V., Lumyong, P., Lumyong, S. & Izumori, K. (2007) Efficient conversion of allitol to D-psicose by *Bacillus pallidus* Y25, *J Biosci Bioeng.* **103**, 282-5.
11. Yoshida, H., Yamada, M., Ohyama, Y., Takada, G., Izumori, K. & Kamitori, S. (2007) The structures of L-rhamnose isomerase from *Pseudomonas stutzeri* in complexes with L-

rhamnose and D-allose provide insights into broad substrate specificity, *J Mol Biol.* **365**, 1505-16.

12. Korndorfer, I. P., Fessner, W. D. & Matthews, B. W. (2000) The structure of rhamnose isomerase from *Escherichia coli* and its relation with xylose isomerase illustrates a change between inter and intra-subunit complementation during evolution, *J Mol Biol.* **300**, 917-33.
13. Meng, M., Bagdasarian, M. & Zeikus, J. G. (1993) The role of active-site aromatic and polar residues in catalysis and substrate discrimination by xylose isomerase, *Proc Natl Acad Sci U S A.* **90**, 8459-63.
14. Siddiqui, K. S., Loviny-Anderton, T., Rangarajan, M. & Hartley, B. S. (1993) Arthrobacter D-xylose isomerase: chemical modification of carboxy groups and protein engineering of pH optimum, *Biochem J.* **296**(Pt 3), 685-91.
15. Sriprapundh, D., Vieille, C. & Zeikus, J. G. (2000) Molecular determinants of xylose isomerase thermal stability and activity: analysis of thermozymes by site-directed mutagenesis, *Protein Eng.* **13**, 259-65.
16. Karimaki, J., Parkkinen, T., Santa, H., Pastinen, O., Leisola, M., Rouvinen, J. & Turunen, O. (2004) Engineering the substrate specificity of xylose isomerase, *Protein Eng Des Sel.* **17**, 861-9.
17. Whitlow, M., Howard, A. J., Finzel, B. C., Poulos, T. L., Winborne, E. & Gilliland, G. L. (1991) A metal-mediated hydride shift mechanism for xylose isomerase based on the 1.6 A *Streptomyces rubiginosus* structures with xylitol and D-xylose, *Proteins.* **9**, 153-73.
18. Fenn, T. D., Ringe, D. & Petsko, G. A. (2004) Xylose isomerase in substrate and inhibitor michaelis states: atomic resolution studies of a metal-mediated hydride shift, *Biochemistry.* **43**, 6464-74.

19. Kovalevsky, A. Y., Hanson, L., Fisher, S. Z., Mustyakimov, M., Mason, S. A., Forsyth, V. T., Blakeley, M. P., Keen, D. A., Wagner, T., Carrell, H. L., Katz, A. K., Glusker, J. P. & Langan, P. Metal ion roles and the movement of hydrogen during reaction catalyzed by D-xylose isomerase: a joint x-ray and neutron diffraction study, *Structure.* **18**, 688-99.

20. Lambeir, A. M., Lauwereys, M., Stanssens, P., Mrabet, N. T., Snauwaert, J., van Tilbeurgh, H., Matthyssens, G., Lasters, I., De Maeyer, M., Wodak, S. J. & et al. (1992) Protein engineering of xylose (glucose) isomerase from *Actinoplanes missouriensis*. 2. Site-directed mutagenesis of the xylose binding site, *Biochemistry.* **31**, 5459-66.

21. Jenkins, J., Janin, J., Rey, F., Chiadmi, M., van Tilbeurgh, H., Lasters, I., De Maeyer, M., Van Belle, D., Wodak, S. J., Lauwereys, M. & et al. (1992) Protein engineering of xylose (glucose) isomerase from *Actinoplanes missouriensis*. 1. Crystallography and site-directed mutagenesis of metal binding sites, *Biochemistry.* **31**, 5449-58.

22. van Tilbeurgh, H., Jenkins, J., Chiadmi, M., Janin, J., Wodak, S. J., Mrabet, N. T. & Lambeir, A. M. (1992) Protein engineering of xylose (glucose) isomerase from Actinoplanes missouriensis. 3. Changing metal specificity and the pH profile by site-directed mutagenesis, *Biochemistry.* **31**, 5467-71.

23. Janis, J., Pasanen, S., Rouvinen, J. & Vainiotalo, P. (2008) Characterization of the pH-dependent dissociation of a multimeric metalloprotein *Streptomyces rubiginosus* xylose isomerase by ESI FT-ICR mass spectrometry, *J Mass Spect.* **43**, 1376-80.

24. Kovalevsky, A. Y., Hanson, B. L., Mason, S. A., Yoshida, T., Fisher, S. Z., Mustyakimov, M., Forsyth, V. T., Blakeley, M. P., Keen, D. A. & Langan, P. (2011) Identification of the elusive hydronium ion exchanging roles with a proton in an enzyme at lower pH values, *Angewandte Chemie.* **50**, 7520-3.

25. Waltman, M. J., Yang, Z. K., Langan, P., Graham, D. E. & Kovalevsky, A. (2014) Engineering acidic *Streptomyces rubiginosus* D-xylose isomerase by rational enzyme design, *Protein Eng Des Sel.* **27**, 59-64.

26. Prabhu, P., Doan, T. T., Jeya, M., Kang, L. W. & Lee, J. K. Cloning and characterization of a rhamnose isomerase from Bacillus halodurans, *Appl Microbiol Biotechnol.* **89**, 635-44.

27. Tiwari, M. K., Singh, R. K., Singh, R., Jeya, M., Zhao, H. & Lee, J. K. (2012) Role of conserved glycine in zinc-dependent medium chain dehydrogenase/reductase superfamily, *J Biol Chem.* **287**, 19429-39.

28. Yoshida, H., Yamaji, M., Ishii, T., Izumori, K. & Kamitori, S. Catalytic reaction mechanism of *Pseudomonas stutzeri* L-rhamnose isomerase deduced from X-ray structures, *FEBS J.* **277**, 1045-57.

29. Lee, D. W., Choe, E. A., Kim, S. B., Eom, S. H., Hong, Y. H., Lee, S. J., Lee, H. S., Lee, D. Y. & Pyun, Y. R. (2005) Distinct metal dependence for catalytic and structural functions in the L-arabinose isomerases from the mesophilic *Bacillus halodurans* and the thermophilic *Geobacillus stearothermophilus*, *Arch Biochem Biophy.* **434**, 333-43.

30. Fuxreiter, M., Bocskei, Z., Szeibert, A., Szabo, E., Dallmann, G., Naray-Szabo, G. & Asboth, B. (1997) Role of electrostatics at the catalytic metal binding site in xylose isomerase action: Ca(2+)-inhibition and metal competence in the double mutant D254E/D256E, *Proteins.* **28**, 183-93.

31. Gao, E. Q., Bai, S. Q., He, Z. & Yan, C. H. (2005) Tetramanganese(II) cluster with centered trigonal topology: structure and magnetic properties, *Inorg Chem.* **44**, 677-82.

32. Ni, C., Fettinger, J. C., Long, G. J. & Power, P. P. Terphenyl substituted derivatives of manganese(II): distorted geometries and resistance to elimination, *Dalton Trans.* **39**, 10664-70.

33. Ni, C., Rekken, B., Fettinger, J. C., Long, G. J. & Power, P. P. (2009) Two-coordinate, homoleptic manganese(II) primary terphenyl amido complexes: the effects of secondary coordination on geometry and Lewis base complexation, *Dalton Trans*, 8349-55.

34. Wang, K., Wang, Y. Q., Zhang, X. M. & Gao, E. Q. Ferromagnetic interactions through double hydrogen bonding bridges in manganese(ii) coordination polymers, *Dalton Trans*.

35. Soisson, S. M., MacDougall-Shackleton, B., Schleif, R. & Wolberger, C. (1997) Structural basis for ligand-regulated oligomerization of AraC, *Science.* **276**, 421-5.

36. Collyer, C. A., Henrick, K. & Blow, D. M. (1990) Mechanism for aldose-ketose interconversion by D-xylose isomerase involving ring opening followed by a 1,2-hydride shift, *J Mol Biol.* **212**, 211-35.

37. Emerson, J. P., Wagner, M. L., Reynolds, M. F., Que, L., Jr., Sadowsky, M. J. & Wackett, L. P. (2005) The role of histidine 200 in MndD, the Mn(II)-dependent 3,4-dihydroxyphenylacetate 2,3-dioxygenase from *Arthrobacter globiformis* CM-2, a site-directed mutagenesis study, *J Biol Inorg Chem.* **10**, 751-60.

38. Zhao, M., Zen, K. C., Hubbell, W. L. & Kaback, H. R. (1999) Proximity between Glu126 and Arg144 in the lactose permease of *Escherichia coli*, *Biochemistry.* **38**, 7407-12.

39. Whiting, A. K., Boldt, Y. R., Hendrich, M. P., Wackett, L. P. & Que, L., Jr. (1996) Manganese(II)-dependent extradiol-cleaving catechol dioxygenase from *Arthrobacter globiformis* CM-2, *Biochemistry.* **35**, 160-70.

40. Angerhofer, A., Moomaw, E. W., Garcia-Rubio, I., Ozarowski, A., Krzystek, J., Weber, R. T. & Richards, N. G. (2007) Multifrequency EPR studies on the Mn(II) centers of oxalate decarboxylase, *J Phys Chem B.* **111**, 5043-6.

41. Rivas-Pardo, J. A., Caniuguir, A., Wilson, C. A., Babul, J. & Guixe, V. Divalent metal cation requirements of phosphofructokinase-2 from *E. coli*. Evidence for a high affinity binding site for Mn^{2+}, *Arch Biochem Biophy.* **505**, 60-6.

42. Samanta, U., Pal, D. & Chakrabarti, P. (2000) Environment of tryptophan side chains in proteins, *Proteins.* **38**, 288-300.

43. Samanta, U. & Chakrabarti, P. (2001) Assessing the role of tryptophan residues in the binding site, *Protein Eng.* **14**, 7-15.

44. DiTusa, C. A., McCall, K. A., Christensen, T., Mahapatro, M., Fierke, C. A. & Toone, E. J. (2001) Thermodynamics of metal ion binding. 2. Metal ion binding by carbonic anhydrase variants, *Biochemistry.* **40**, 5345-51.

45. Brodkin, H. R., Novak, W. R., Milne, A. C., D'Aquino, J. A., Karabacak, N. M., Goldberg, I. G., Agar, J. N., Payne, M. S., Petsko, G. A., Ondrechen, M. J. & Ringe, D. (2011) Evidence of the participation of remote residues in the catalytic activity of Co-type nitrile hydratase from *Pseudomonas putida*, *Biochemistry.* **50**, 4923-35.

46. Alam, A., Shi, N. & Jiang, Y. (2007) Structural insight into Ca^{2+} specificity in tetrameric cation channels, *Proc Natl Acad Sci U S A.* **104**, 15334-9.

47. He, Q. Y., Mason, A. B., Lyons, B. A., Tam, B. M., Nguyen, V., MacGillivray, R. T. & Woodworth, R. C. (2001) Spectral and metal-binding properties of three single-point tryptophan mutants of the human transferrin N-lobe, *Biochem J.* **354**, 423-9.

48. Ataie, N. J., Hoang, Q. Q., Zahniser, M. P., Tu, Y., Milne, A., Petsko, G. A. & Ringe, D. (2008) Zinc coordination geometry and ligand binding affinity: the structural and kinetic analysis of the second-shell serine 228 residue and the methionine 180 residue of the aminopeptidase from *Vibrio proteolyticus*, *Biochemistry.* **47**, 7673-83.

49. Bradford, M. M. (1976) A rapid and sensitive method for the quantitation of microgram quantities of protein utilizing the principle of protein-dye binding, *Anal Biochem.* **72**, 248-54.

50. Dische, Z. & Borenfreund, E. (1951) A new spectrophotometric method for the detection and determination of keto sugars and trioses, *J Biol Chem.* **192**, 583-7.

51. Doan, T. N., Prabhu, P., Kim, J. K., Ahn, Y. J., Natarajan, S., Kang, L. W., Park, G. T., Lim, S. B. & Lee, J. K. Crystallization and preliminary X-ray crystallographic analysis of L-rhamnose isomerase with a novel high thermostability from *Bacillus halodurans*, *Acta Crystallogr Sect F Struct Biol Cryst Commun.* **66**, 677-80.

52. Minor, W., Steczko, J., Bolin, J. T., Otwinowski, Z. & Axelrod, B. (1993) Crystallographic determination of the active site iron and its ligands in soybean lipoxygenase L-1, *Biochemistry.* **32**, 6320-3.

53. Vagin, A. & Teplyakov, A. (1998) A translation-function approach for heavy-atom location in macromolecular crystallography, *Acta Crystallogr D Biol Crystallogr.* **54**, 400-2.

54. Laskowski, R. A., Moss, D. S. & Thornton, J. M. (1993) Main-chain bond lengths and bond angles in protein structures, *J Mol Biol.* **231**, 1049-67.

55. Tiwari, M. & Lee, J. K. (2010) Molecular modeling studies of L-arabinitol 4-dehydrogenase of *Hypocrea jecorina*: its binding interactions with substrate and cofactor, *J Mol Graph Model.* **28**, 707-13.

Supporting Information

Fig. S1. Structure-based sequence alignment of L-RhIs from *Bacillus halodurans*, *E. coli* and *Pseudomonas stutzeri*. Conserved residues are shown in dark blue background; semi-conserved residues are shown in grey background. The figure was generated using Materials Studio 5.5 program.

Fig. S2. Multiple sequence alignment of BHRI with other L-rhamnose isomerases and two metal dependent isomerases; xylose isomerases and glucose isomerases. Conserved amino acids are shown as black letters in pink background. W38 is well conserved throughout the family and is indicated with an asterisk. Xylose isomerases: GTXI, *Geobacillus thermodenitrificans* (A4IP67); BHXI, *Bacillus halodurans* (NP_243623.1); BSXI, *Bacillus subtilis* (P04788); BLXI, *Bacillus licheniformis* (P77832); LBXI, *Lactobacillus brevis* (Q03TX3); TNXI, *Thermotoga neapolitana* (P45687); TMXI, *Thermotoga maritima* (Q9X1Z5); ECXI, *Escherichia coli* (B1IZM7); STXI, *Salmonella typhimurium* (Q8ZL90); SRXI, *Streptomyces rubiginosus* (P24300). L-Rhamnose isomerases: ECRI, *Escherichia coli* (B5YZ40); SDyRI, *Shigella dysenteriae* (B3X1L6); SERI, *Salmonella enterica* (B5P7I1); STRI, Salmonella typhimurium (P27031); KPRI, *Klebsiella pneumonia* (B5XZ52);YPRI *Yersinia pestis* (A4TRT1); BSRI *Bacillus subtilis* (O05264); OIRI, *Oceanobacillus iheyensis* (Q8ESX0); BHRI, *Bacillus halodurans* (Q9KCL9); GSRI, *Geobacillus sp.* (B3KJL8). Glucose isomerases: BCGI, *Bacillus coagulans* (ZP_04430850.1); FGGI, *Fervidobacterium gondwanense* (AAR07504.1); SAGI, *Streptomyces albus* (P24299); SMGI, *Streptomyces murinus* (CAA00885.1); AMGI, *Actinoplanes missouriensis* (CAA00884.1). The BHRI sequence is indicated by arrows in the left.

Fig. S3. Conserved residues (pink) around the catalytic amino acids and metal ion binding residues (brown) selected for site-directed mutagenesis analysis.

Fig. S4. Wall-eye stereoview of metal binding sites of the wild-type (apo) structure, wild-type-Mn structure, W38F-Mn structure, and W38A-Mn structure with their refined maps. The blue map shows a 2Fo-Fc map contoured at 1.0σ, and the green map shows a Fo-Fc map contoured at 3.0σ. The view orientations are identical to that of Figure 3 and Figure 4.

Fig. S5. Metal-ion-binding pocket in mutant W38A-Mn and wild-type BHRI (apo). (A) Two water molecules were bound at the metal binding site of BHRI W38A structure. A Mn ion was bound in only a monomer of a tetramer in asymmetric unit. (B) A water molecule was bound at the metal binding site of wild-type BHRI structure.

Fig. S6. Comparison of substrate binding pockets in crystal structure of L-RhI (rhamnose isomerase) and homology model of XI (xylose isomerase). (A) Substrate binding pocket of BHRI-Mn with W38 nearby structural metal ion binding residue D325. Amino acids colored by element. (B) Substrate binding pocket of BLXI (*Bacillus licheniformis*, xylose isomerase) with W47 nearby D337. Amino acids are colored aqua. Metal ions M1 and M2 are shown in purple.

Fig. S7. Mn^{2+} binding as assessed by EPR for wild-type BHRI (grey line) and the W38F mutant (black line).

Table 1. X-ray data collection and refinement statistics for obtained BHRI and W38 mutants

Data collection	**Apo enzyme**	**BHRI-Mn**	**W38F-Mn**	**W38A**
X-ray source	6C1- PLS	4A- PLS	4A- PLS	4A- PLS
Space group	$P2_1$	$P2_1$	$P2_1$	$P2_1$
Wavelength	1.24	1.00	1.00	1.00
Resolution (Å)	50.0-2.59 (2.64-2.59)	50.0-2.8 (2.85-2.80)	50-2.7 (2.75-2.70)	50-2.75 (2.80-2.75)
Cell dimensions	a = 83.2 Å, b = 164.9 Å, c = 92.0 Å, α=γ=90°, β= 116°	a = 83.6 Å, b = 165.6 Å, c = 92.5 Å, α=γ=90°, β= 116°	a = 83.4 Å, b = 164.8 Å, c = 92.8 Å, α=γ=90°, β= 117°	a = 83.4 Å, b = 164.8 Å, c = 92.8 Å, α=γ=90°, β= 117°
No. of observed reflections (unique)	212,685 (72,032)	166,370 (56,522)	166,804 (53,466)	150,071 (50,338)
Completeness (%)	98.0 (99.6)	96.0 (98.4)	88.3 (91.2)	79.0 (82.5)
R_{sym} [†] (%)	9.1 (44.2)	9.5 (41.2)	10.8 (43.1)	11.1 (39.0)
Average I/σ(I)	13.1 (2.6)	14.1 (3.0)	11.8 (2.5)	10.3 (2.3)
Refinement				
Resolution (Å)	45.78 (2.60)	46.62 (2.80)	45.87 (2.70)	45.87 (2.75)
Number of reflection	70,988	56,461	51,528	46,347
(Working/Free R set)	3,751	3,022	2,778	2,480
R/R_{free} factor (%)	18.9/25.5 (26/34)	18.4/25.5 (27/35)	19.0/26.6 (26/35)	19.0/26.6 (27/38)
Number of residues	Mol-A 400 Mol-B 401 Mol-C 400 Mol-D 399	Mol-A 402 Mol-B 401 Mol-C 401 Mol-D 404	Mol-A 401 Mol-B 403 Mol-C 404 Mol-D 403	Mol-A 402 Mol-B 402 Mol-C 404 Mol-D 404
Waters	451	318	484	263
B-factor ($Å^2$)	32.4	33.0	32.8	31.5
Protein	35.0	35.6	35.4	34.5
Water	31.7	30.6	29.0	25.2
Metal	n/a	49.5	67.0	71.6[a]
RMS bond lengths (Å)	0.019	0.017	0.015	0.014
RMS bond angles(°)	1.825	1.778	1.694	1.663
Ramachandran plot (%)				
Mostfavored	94.70	93.50	93.00	92.42
Allowed	4.46	5.70	5.75	5.6
Generous	0.84	0.80	1.25	1.98

[†] $R_{sym} = \Sigma_{hkl}\Sigma_i|I_i(hkl) - \langle I(hkl)\rangle| / \Sigma_{hkl}\Sigma_i I_i(hkl)$, where $I(hkl)$ is the intensity of reflection hkl, Σ_{hkl} is the sum over all reflections and Σ_i is the sum over i measurements of reflection hkl. N is redundancy of the measurement of reflection hkl. Values in parentheses are for the highest resolution shell. [a] In the four protomers of W38A tetramer, there was only one Mn ion bound. Each protomer of wild type and W38F tetramers had two Mn ions at the active site.

Table 2. Kinetic parameters determined for wild-type BHRI and mutants

Enzyme	K_m (mM)	k_{cat} (min^{-1})	k_{cat}/K_m ($mM^{-1}min^{-1}$)	$\Delta\Delta G^a$ (kJ mol^{-1})
Wild-type	528 ± 14	8970 ± 130	17.0 ± 0.7	0
N182A	535 ± 19	8970 ± 150	16.7 ± 0.9	0.05
N131A	564 ± 17	8400 ± 140	14.8 ± 0.7	0.39
F327A	578 ± 21	8210± 170	14.2 ± 0.8	0.51
H36A	580 ± 27	7920 ± 180	13.6 ± 0.9	0.63
W184A	805 ± 43	2640 ± 50	3.20 ± 0.22	4.76
W292A	986 ± 46	960 ± 37	0.97 ± 0.08	8.16
W38A	ND	ND	ND	ND

The k_{cat} values were calculated by considering the enzyme as a monomer.
Results are means ± S.D. for three experiments.
[a]$\Delta(\Delta G) = -RT \ln[(k_{cat}/K_m)\text{mut}/(k_{cat}/K_m)\text{wt}]$, where mut is mutant and wt is wild-type, R is ideal gas constant and T is the temperature.
ND - Not detected due to very low activity.

Table 3. Thermodynamic parameters determined for wild-type BHRI and mutant with Mn^{2+}

Enzyme	n	K_d (μM)	ΔG (kJ mol^{-1})	TΔS	ΔH
BHRI	8.20 ± 0.07	1.57 ± 0.2	-33.1 ± 0.9	4.81 ± 0.03	-28.3 ± 0.8
W38F	6.31 ± 0.05	8.14 ± 0.1	-29.0 ± 0.5	6.64 ± 0.02	-22.4 ± 0.5
W38A	0.87 ± 0.11	732 ± 6	-17.9 ± 0.6	7.19 ± 0.04	-10.7 ± 0.7

Titrations were carried out at 25°C.
Gibbs free energy (ΔG) and entropy (ΔS) were calculated using the fundamental equations: $\Delta G = -RT \ln K$ and $\Delta S = (\Delta H - \Delta G)/T$.

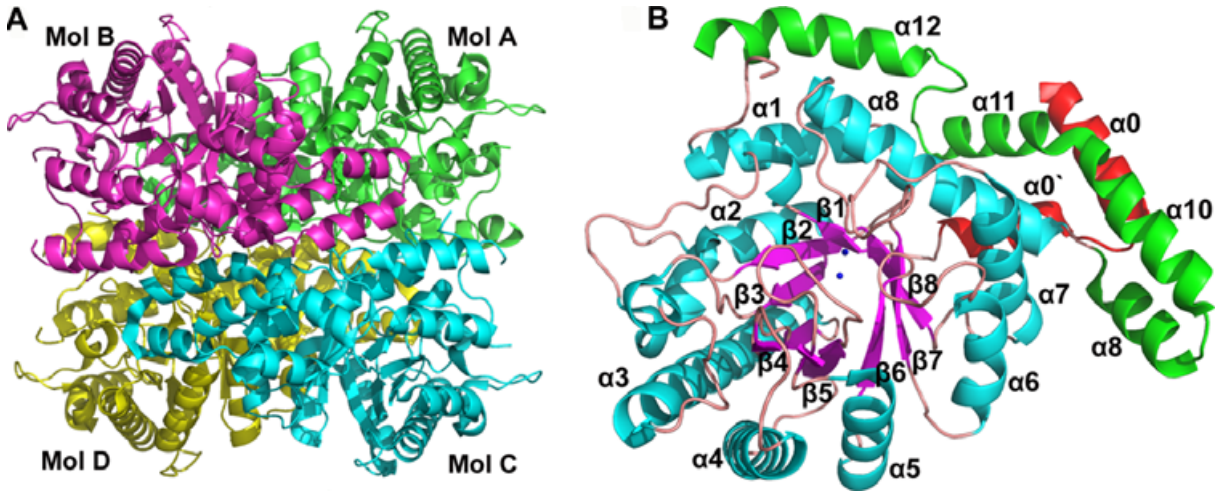

Figure 1. Structure of BHRI. (A) BHRI forms a tetramer, as shown. Subunits A, B, C, and D are represented in green, magenta, cyan, and yellow, respectively. (B) The BHRI monomer is composed of one large domain with 8 cyan α-helices and 8 magenta β-sheets and one small domain with α-helices at the N-terminus and a red α-helix at the C-terminus.

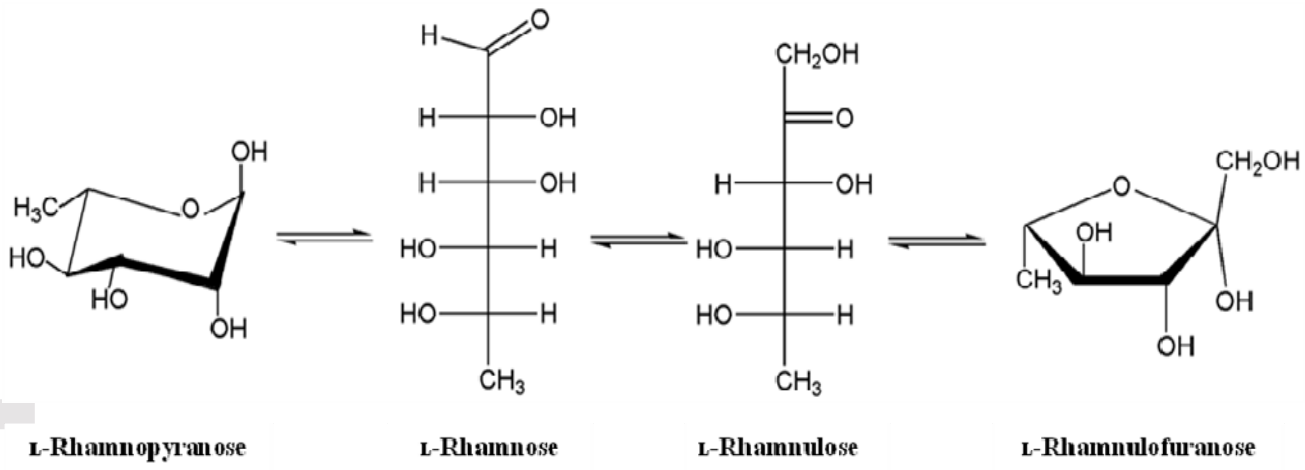

Figure 2. Scheme of the reaction catalyzed by *B. halodurans* L-RhI. The possible reaction mechanism is suggested based on the mechanism of *E. coli* L-RhI [12].

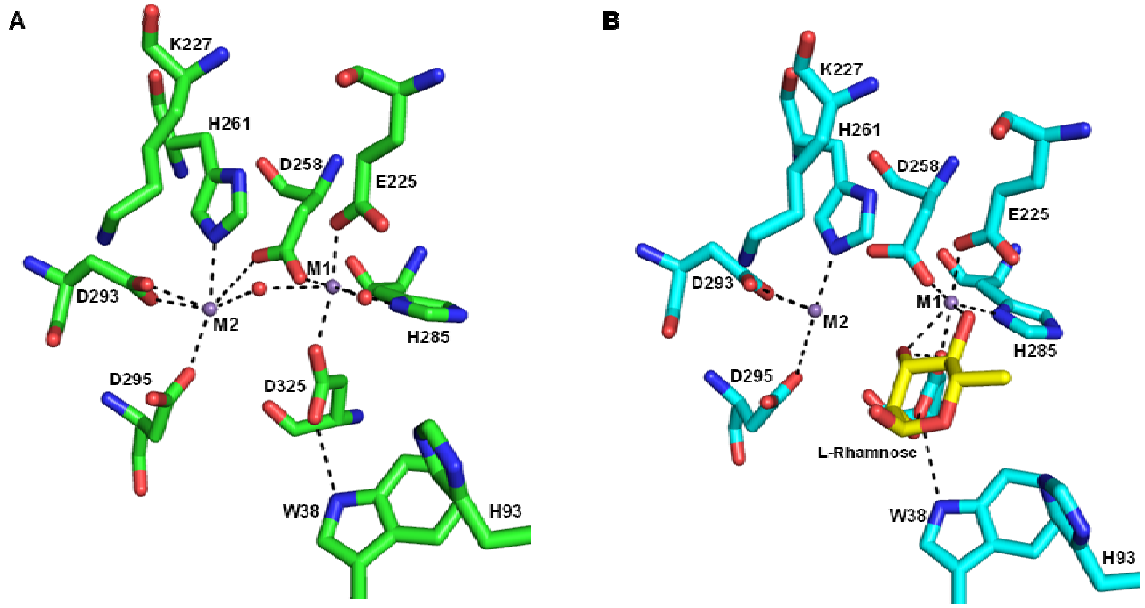

Figure 3. Metal-ion-binding pocket in wild-type BHRI-Mn. (A) Structural metal ion (M1) in its respective position, showing octahedral geometric coordination, forming six coordination bonds from four structural metal-ion-binding residues and two water molecules. (B) When cyclic L-rhamnose was docked into BHRI-Mn (BHRI-Mn-CyclicRham), proper interactions occurred with the structural metal ion (M1) and M1-binding residue, D325. Active site residues, metal ions, and L-rhamnose are shown cyan, purple, and yellow, respectively. Carbon atoms C3 and C4 of L-rhamnose are in proper positions, with M1 coordinating with O3 and O4. The black dotted lines represent the metal coordinations and H-bonds in the active site.

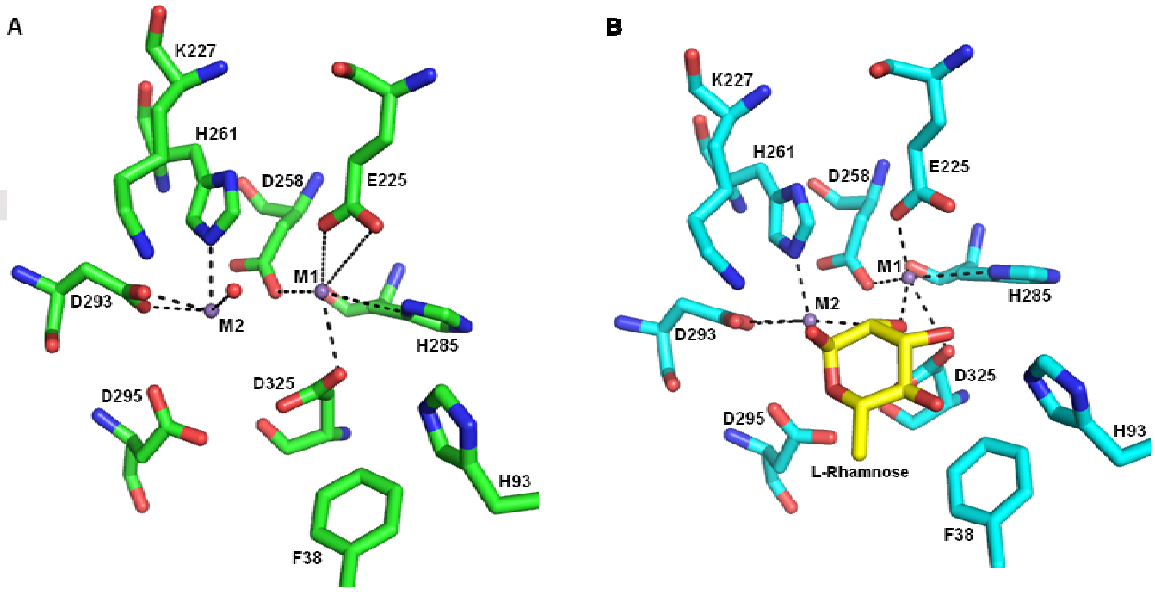

Figure 4. Metal-ion-binding pocket in mutant W38F-Mn. (A) M1 metal ion forms only four coordination bonds with M1-binding residues showing increased distances between each residue

and the metal ion M1 compared with the wild-type enzyme. (B) Cyclic L-rhamnose substrate in the W38F-Mn structure is not in the proper orientation to interact with M1. L-Rhamnose is coordinated to M1 in BHRI-Mn-CyclicRham, where O3 and O4 of the substrate are far from M1 with the distance of 3.6Å and 6.4Å, respectively. Active site residues, metal ions, and L-rhamnose are shown cyan, purple, and yellow, respectively. The black dotted lines represent the metal coordinations and H-bonds in the active site.

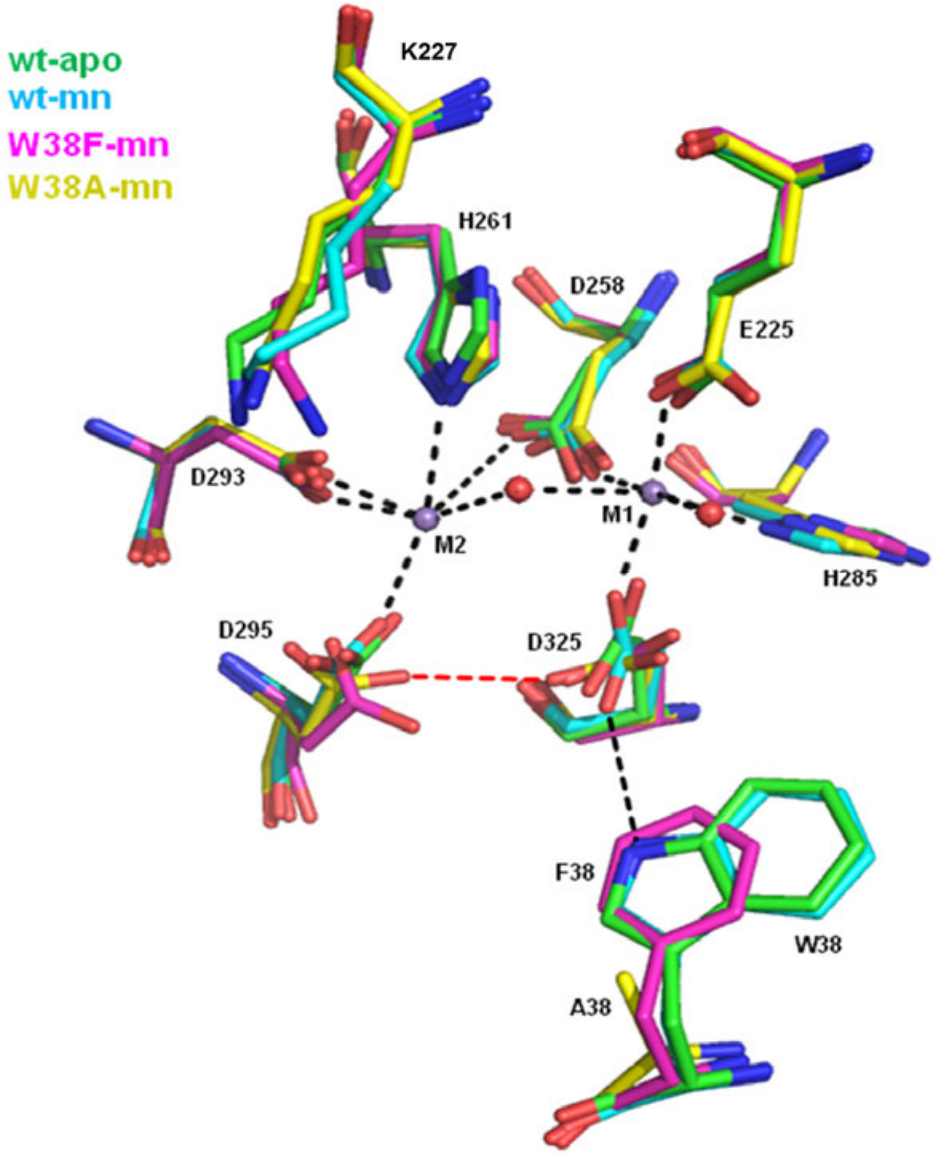

Figure 5. Superimposed structures of BHRI wild-type-apo (green), wild-type-Mn (cyan), W38F-Mn (purple), and W38A-Mn (yellow). In the wild-type-Mn structure, metal, and water molecules, including their coordination (black dashed line) are shown. The red dashed lines represent the hydrogen bonds between D295 and D325 in W38F and W38A structures.

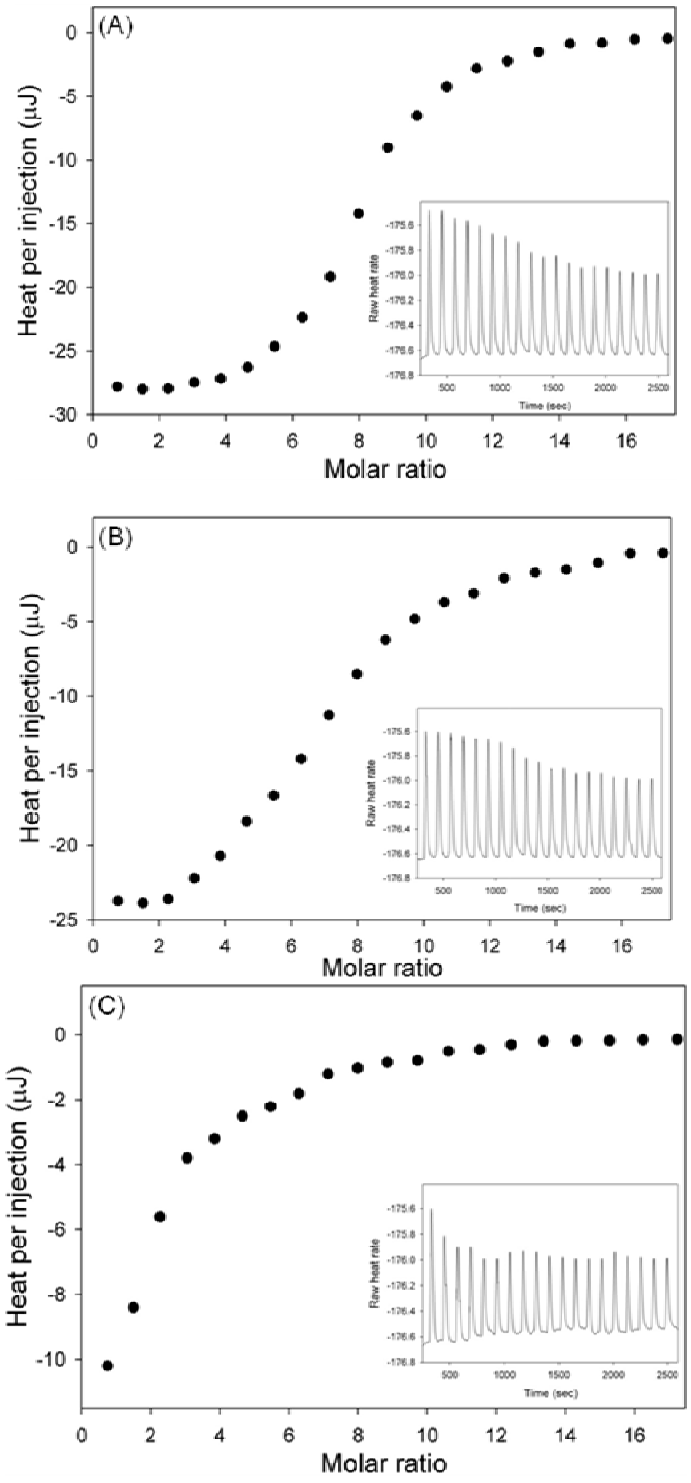

Figure 6. Isothermal titration calorimetry trace for the binding of Mn^{2+} to wild-type BHRI (A), W38F mutant (B) and W38A mutant (C). The graph shows the integrated areas of the heat absorbed along with a fit from which the molar association constant (*K*), enthalpy (ΔH), and entropy (ΔS) were calculated. The inset shows the thermogram.